PCCP

RSC Publishing

PERSPECTIVE

View Article Online
View Journal | View Issue

The role of interfacial charge transfer-type interactions in the decay of plasmon excitations in metal nanoparticles

Cite this: *Phys. Chem. Chem. Phys.*, 2013, **15**, 7441

Kenneth O. Aruda, Mario Tagliazucchi, Christina M. Sweeney, Daniel C. Hannah and Emily A. Weiss*

Received 6th March 2013,
Accepted 11th April 2013

DOI: 10.1039/c3cp51005k

www.rsc.org/pccp

This perspective describes the influence of interfacial charge transfer-type interactions on the optical spectra and hot electron cooling processes in plasmonic nanoparticles (NPs), and ongoing work to optimize these interactions for charge extraction from the plasmon or hot electron state. The manuscript focuses on interfaces of metal NPs with organic molecules and with semiconductors. Charge extraction from multi-electron excited states has applications in photodetection, sensing, and conversion of solar energy to electricity and fuels.

Introduction

This perspective article discusses the current understanding of the role of interfacial charge-transfer type interactions in the decay of plasmon excitations in metal nanoparticles, and the implications of these interactions for charge extraction from photoexcited states. Currently, a ''plasmonic solar cell'' usually refers to a device in which plasmonic NPs increase the yield of light absorption in photovoltaic active materials by trapping and scattering the light at the surface, and thereby increasing the effective path length of the material. Plasmonic NPs are, in principle, also appealing as active materials (materials that absorb light and create mobile charge carriers) themselves because plasmons are high-oscillator strength, multi-electron excitations with resonance wavelengths that span high-flux portions of the solar spectrum (350–750 nm).[1] NPs are not currently widely employed in solar cells as the active material because the excited electrons dissipate their energy as heat within a few picoseconds, which makes excited state decay competitive with interfacial charge transfer (CT),[2,3] and because the principles that dictate extraction of charge carriers are not yet as well-defined for metal NPs as for molecules or semiconductor quantum dots (QDs).[4] Recently, charge transfer-type interactions, where hot electrons transiently occupy the orbitals of chemisorbed ligands, have been described in colloidal Au NPs.[2,5–10] These interactions are interesting and potentially useful with respect to solar energy conversion, because they affect the dynamics of plasmon relaxation. Chemical control of the rate of plasmon decay through surface chemistry influences the probability of charge extraction from the hot electron state in two ways: (i) interaction with ligands may slow the electron cooling dynamics such that charge extraction occurs faster than carrier cooling, and (ii) the charge-transfer type interactions that influence decay rates may also serve as pathways to localize charge carriers on proximate redox-active ligands.

Department of Chemistry, Northwestern University, 2145 Sheridan Rd., Evanston, IL 60208-3113, USA. E-mail: e-weiss@northwestern.edu; Fax: +1 847-491-7713; Tel: +1 847-491-3095

The plasmon decay process

After light absorption, the plasmon dissipates its energy through three types of processes that have distinct timescales such that, in the simplest model of carrier cooling, the processes occur sequentially. In the first phase, hot electrons lose coherence and energy by scattering with other electrons within the metal lattice, or electrons in interfacial orbitals. Electron–electron scattering occurs on a timescale of hundreds of femtoseconds,[11–17] after which the electrons at the Fermi level have equilibrated with one another, and can be thought of as an electron bath with a single temperature. In the second phase, hot electrons cool by distributing energy into directly coupled vibrational modes. Over the course of approximately 10 picoseconds, the electrons undergo inelastic scattering with phonon and vibrational modes to heat the metal lattice and, possibly, the ligands. Throughout this manuscript, this scattering time is referred to as the ''hot electron lifetime''. In the third phase, the hot lattice phonons and ligand vibrations thermally equilibrate with the solvent, or other surrounding matrix. This process occurs in hundreds of picoseconds; its rate depends strongly on the heat capacities of the nanoparticle and its matrix (Fig. 1).

The power-dependent lifetime of hot electrons created by excitation at the plasmon resonance has been described in the

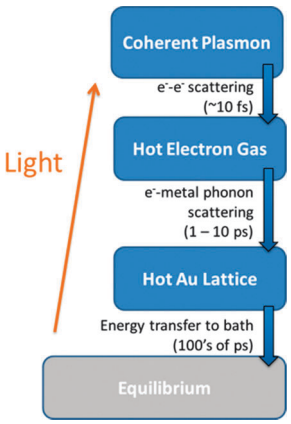

Fig. 1 The progressive dissipation of energy from a plasmonic NP. Nonradiative decay of a plasmon leads to the production of a ''hot'' (thermalized) electron gas. The hot electrons couple to the vibrational modes of the metal lattice and possibly coordinated ligands, which in turn dissipate energy to the local environment of the NP.

literature with a ''two temperature model (2TM)''. The general form of the 2TM is given by the differential eqn (1) and (2). From eqn (1) and (2), the change in electronic temperature (T_e) and the lattice temperature (T_L) in time depends on the electronic heat

$$\gamma T_e \frac{dT_e}{dt} = -g(T_e - T_L) \quad (1)$$

$$C_L \frac{dT_L}{dt} = g(T_e - T_L) \quad (2)$$

capacity coefficient, γ, the electron–phonon coupling magnitude g, and the heat capacity of the lattice, C_L. If we assume that T_L remains constant throughout the cooling process (due to the large heat capacity of the lattice compared to that of the electrons), T_e decays with first order kinetics with a characteristic lifetime τ (eqn (3)), which increases with increasing initial electron temperature (ΔT_e^{max}), and depends on the initial temperature of the system (T_0). The hot electron lifetime τ is, by definition, a power-dependent decay time.

$$\tau = \frac{\gamma(T_0 + \Delta T_e^{max})}{g} = \frac{\tau T_0}{g} + \frac{\gamma \Delta T_e^{max}}{g} \quad (3)$$

A power-independent hot electron lifetime, τ_0, is normally determined by measuring the hot electron lifetimes at several excitation powers, and then extrapolating to the lifetime at zero power.

There are three major potential complications in using the 2TM to determine the electronic heat capacity and electron–phonon coupling magnitude of an NP–ligand system: (i) the model assumes that the thermalization of electrons and phonons occurs sequentially; however, if the timescales of these processes overlap, the coupled differential equations become significantly more complicated.[18] This issue is ameliorated by limiting the range of the measured cooling dynamics to times when the electron temperature is much larger than the lattice temperature. (ii) The relationship between ΔA (the differential absorption in the region of the plasmon resonance) and the increase in electronic temperature upon photoexcitation, ΔT_e, varies with NP size and surface chemistry, and is not necessarily linear. A strategy for addressing this issue is to fit the differential absorption spectrum at a given time after photoexcitation, using the dielectric model from Rosei *et al.*[19] and Inouye *et al.*,[17] to extract an electronic temperature at that time, rather than assuming that $\Delta A \propto \Delta T_e$. Such a fit of the differential absorption spectrum immediately after photoexcitation yields an initial electronic temperature that also allows for determination of the electronic heat capacity. (iii) NPs of different size, shape and surface chemistry have different extinction coefficients, so the hot electron lifetime depends on the laser power only through the expectation value of absorbed photons per NP. In using the 2TM to compare the ''zero-power'' hot electron lifetimes, τ_0, of different samples from lifetimes measured at a series of laser powers, one must account for the relative extinction coefficients of the samples.

If these issues are addressed, the 2TM is a useful model to describe the dependence of hot electron cooling in NPs on their surrounding medium or ligand shell.

Factors that contribute to the linewidth of the steady-state plasmon resonance

The steady-state spectra of isolated nanoparticles and *monodisperse* ensembles of metal nanoparticles are useful for investigating particle size, shape, and the metal/environment interface due to the impact of these factors on the plasmon peak position(s) and the homogeneous linewidth (Γ_{hom}).[20,21] Of particular importance, the dephasing time (t_2), which describes the coherence lifetime of the plasmon, relates directly to Γ_{hom} *via* the equation $t_2 = 2\hbar/\Gamma_{hom}$ and serves as an indication of various damping and scattering mechanisms.[22,23] The radius of the particle (R) will determine the type of damping present in the system.[20,24] For example, radiative damping (conversion of plasmons into photons) is the dominant mechanism when $R \geq 10$ nm, surface scattering/non-radiative damping (electron scattering) dominates when $R < 2$ nm, and both damping mechanisms contribute when $2 < R < 10$ nm.[10,21,22,24–26] The contribution of each damping mechanism to the linewidth is given by eqn (4),[10]

$$\Gamma_{hom} = \Gamma_{bulk} + \Gamma_{nonrad} + \Gamma_{rad} \quad (4)$$

where Γ_{bulk} is the bulk damping constant of the metal and is related to the real and imaginary components of the dielectric function; $\Gamma_{nonrad} = \frac{A\nu_F}{L_{eff}}$ is the contribution of surface scattering where A is a constant, ν_F is the Fermi velocity, and L_{eff} is the effective path length of the conduction electrons; and $\Gamma_{rad} = \frac{h\kappa V}{\pi}$ is the contribution of radiative damping, where h is Planck's constant, κ is an experimentally determined value (fs^{-1} nm^{-3}), and V is the volume of the nanoparticle.

Many factors potentially contribute to linewidth broadening; therefore, several methods have been developed, both theoretical and experimental, to differentiate their relative contributions.

For example, simple ground state absorption experiments coupled with theory were used to analyze Γ_{hom} directly for highly monodisperse silver nanoplate sols to determine the contribution from the assorted damping mechanisms.[27] Although some inhomogeneous broadening (due to small size modulations) was present, the authors were able to determine that radiative damping played only a minor role in Γ_{hom} by observing limited spectral changes with increased edge-length. More sophisticated spectroscopic techniques, such as persistent spectral hole burning, which generates a absorption spectrum of a monodisperse subset of particles in a polydisperse sample, eliminate the contributions of inhomogeneous line-width broadening to Γ_{hom}, and has enabled more detailed investigation of other damping mechanisms.[23] Stietz *et al.*, for example, determined that oblate Ag nanoparticles ($R \sim 7.5$ nm) have a linewidth of 260 meV corresponding to a t_2 of 4.8 fs.[23] This lifetime is shorter than expected for damping by only electron scattering and it was determined that surface scattering mechanisms play a significant role. In addition, particles with high aspect ratios and good monodispersity, such as gold nanorods, can be used to study size effects on Γ_{hom} and for determining likely damping mechanisms.[10,21,26] Novo *et al.* used single-particle absorption measurements to determine that there was a competition between surface scattering and radiative damping based on size; based on this observation it was determined that nanorods with lengths of $L \sim 20$ nm produced the narrowest Γ_{hom} and thus have the least damped plasmons.[10] In comparison to similarly sized gold nanospheres, gold nanorods were also found to have a reduced dephasing rate due to a suppressed interband damping and reduced radiation damping.[21] Temperature variations also differentiate between damping mechanisms in gold bipyramids, where a 30% decrease in Γ_{hom} was observed with decreased temperature, which can be attributed to reduced electron–phonon scattering but not to electron–electron scattering, electron–surface scattering, or radiative relaxation.[26]

In addition to traditional plasmon broadening mechanisms, processes attributed to direct ultrafast nonthermal electron–adsorbate interactions can also decrease the plasmon coherence lifetime and result in larger linewidth. These processes include ultrafast chemical interface scattering (UCIS) and charge transfer. UCIS is an inelastic resonant scattering decay process for nonthermal electrons whereby electrons are scattered into the empty electronic states of NP adsorbates.[28] This mechanism was proposed by Bauer *et al.* to analyze ultrafast decay of excitation in 4.2 nm AuNPs embedded in a sintered TiO_2 matrix. In this study, analysis of transient spectra enabled probing of both the nascent nonthermal electrons (NNEs), formed immediately after photoexcitation, and thermalized electrons.[28] The lifetimes of the NNEs in Au NPs were four times longer than those silver NPs of similar size; the acceleration was attributed to UCIS, which also broadens the plasmon in the steady-state spectrum by enabling a channel for direct transfer of heat to the bath. Charge transfer was again implicated in accelerated excited state decay and broadening of the steady-state plasmon absorbance in a system of gold "nanodots" (10 nm) embedded in TiO_2 films.[29] The observation of metal–adsorbate interactions' influencing the steady-state absorption of metal NPs strongly implies that adsorbates will affect the dissipation dynamics of photoexcited NNEs and that charge transfer from a NNE population is possible.

Dependence of hot electron lifetime on the metal/organic interface

Comparison of literature reports of hot electron lifetimes for NPs suggests that the surrounding matrix or organic adlayer of the NP plays a role in this lifetime. Table 1 lists examples of changes in hot electron lifetimes with changes in the interfacial

Table 1 Reports of changes to the hot electron cooling rates in Au NPs with changes in the surrounding medium

Experimental system	Proposed origin of observed change in hot electron lifetime
Au NPs in acetonitrile *vs.* $MgSO_4$ powder[35]	Dependence on heat capacity of surrounding matrix
Au nanorods and tetrahedra in air *vs.* water[36]	Dependence on heat capacity of surrounding matrix
Au NPs in sol–gel matrix[32,37] *vs.* Au thin films	Dependence on heat capacity of surrounding matrix
Au NPs passivated with amines *vs.* thiolates[42]	Surface chemistry-correlated changes to the electronic DOS and electronic heat capacity
Citrate passivated Au NPs[38] *vs.* thiolate passivated Au NPs[15,54]	Surface chemistry
Au Nanoshells wrapped in poly(vinyl) alcohol[41] *vs.* bare Au NPs	Surface chemistry and dependence on size/shape of NPs
Dissociation of thiol-linked DNA[49] *vs.* citrate passivated Au NPs	Surface chemistry
Citrate Au NPs in water *vs.* oleylamine, and hexanethiol passivated Au NPs in toluene[47]	Surface chemistry
Au NPs coated with polyamidoamine *vs.* hexanethiol[39]	Surface chemistry
Au NPs passivated by sulfates embedded in TiO_2 *vs.* bare Au NPs[2,5–7]	Surface chemistry
Au NPs coated in thiols, thiophenols, amines, or anilines[44]	Surface chemistry
Comparison of Au NPs and Au thin films[32]	Dependence on size/shape of NPs
Shape and aspect ratio dependence of hollow Au nanospheres[40]	Dependence on size/shape of NPs
Aqueous Au NPs[34] of 4–50 nm	Dependence on size/shape of NPs
Au NPs of 9–48 nm *vs.* Au–Ag alloys[31]	No size dependence observed for gold nanoparticles with diameters between 9 and 48 nm.
Au_{55} *vs.* 15 nm Au NPs[30]	Dependence on size of NPs
Polycrystalline *vs.* single crystal Au NPs[53]	Electron phonon coupling dependence on lattice crystallinity

structure of the NP, including that induced by changing the surface area-to-volume ratio through the size and shape. The first three entries in Table 1 report changes in the hot electron lifetimes when the NPs were embedded in media with different heat capacities, such as water, chloroform, gels, or powder films.[30–41] There is a correlation between the heat capacity of the surrounding medium and the hot electron lifetime, as the 2TM predicts; however, a non-coordinating solvent is not directly coupled to the energy of hot electrons, and, within the 2TM, only affects hot electron lifetime indirectly by influencing the dissipation of heat from the metal lattice and coordinating ligands to the solvent.[42] There are also examples where substantial differences in the heat capacity of the solvent produces negligible differences in hot electron lifetime, for example, for hot electrons of NPs in water and heavy water,[43] which have a 12% differences in heat capacity.[43,44] We believe that an equally likely explanation for the correlation between the hot electron lifetime and the heat capacity of a non-coordinating matrix in many of these cases is that changes in media were performed in ways that do not conserve the coordinating surface chemistry of the NPs – that is, they induce a ligand exchange[2,31–33,35,36,38,39,44] or change a variety of factors, including surface chemistry and lattice crystallinity, by annealing the NPs.[35]

A second set of entries in Table 1 report changes in hot electron lifetime upon explicit changes in the surface chemistry of the NP. It is reasonable to expect a dependence of lifetime on surface chemistry because molecules such as fluorophores[45] are known to exchange electrons with metallic surfaces when the metal is photoexcited, and these chemical interface scattering events should give an additional decay pathway for excited electrons. Bauer *et al.*[2,5–7] point out that the ultrafast chemical interface scattering process that was used to explain the differences in the width of the plasmon resonances of small chemically functionalized nanoparticles changes the initial thermalization rates of plasmonic electrons. This result suggests that electrons in the metallic and organic components rapidly equilibrate during the timescale of initial electron thermalization, and that this mixing affects subsequent hot electron cooling.

There are two parameters through which organic ligands modulate the hot electron cooling rate: the electronic heat capacity of the system, and the magnitude of the electron–phonon coupling. The electronic heat capacity influences the hot electron lifetime in two ways: (i) the electronic heat capacity determines the initial temperature of the electrons created in Au NP by a photon, and therefore mediates the initial difference in temperature between the electrons and phonons upon light absorption. (ii) The instantaneous rate of cooling is proportional to the electronic heat capacity. The electronic heat capacity has generally been assumed to have the same value in small NPs as in the bulk,[11–15,17,41] which is only a reasonable assumption if the NP electronic density of states (DOS) is identical to that of the bulk DOS. Eqn (5) is the semiclassical expression that relates

$$C_e(T_e) = \int_{-\infty}^{\infty} \frac{df(\varepsilon, \mu, T_e)}{dT_e} \mathrm{DOS}(\varepsilon)\varepsilon \, d\varepsilon \qquad (5)$$

the electronic heat capacity, $C_e(T_e)$ and the electronic DOS of the NP–ligand system, where the function $f(\varepsilon, \mu, T_e)$ is the Fermi–Dirac distribution as a function of energy (ε), chemical potential (μ) and electronic temperature (T_e). At low electronic temperatures, eqn (5) reduces to the more intuitive eqn (6), where $C_e(T_e)$ depends linearly on the electronic DOS at the Fermi level.

$$C_e(T_e) = \gamma T_e; \quad \gamma = \frac{1}{3}\pi^2 {k_B}^2 \mathrm{DOS}(\varepsilon_{\mathrm{fermi}}) \qquad (6)$$

Note that, for metals, the electronic states at the Fermi level will mix with those of organic adsorbates, so the DOS of passivated metal NPs will differ from bulk DOS. For instance, Au NPs passivated with thiolates have additional states at the Fermi level due to mixing of the electronic states of thiolates with those of the Au core.[46] When organic ligands bind to metal NPs, the electronic heat capacity therefore can be significantly altered from that of the bulk.

There are several literature reports of altered hot electron cooling rates upon adsorption/exchange of amines,[37,42,47] anilines,[44] citrate,[8,47,48] sulfonates,[2,5] and thiols.[42,44,49] Some publications do not report on a specific mechanism for the changes in the hot electron cooling rate, but all of these molecules are coordinating ligands, and therefore alter the electronic DOS at the metal/organic interface. Halas and coworkers showed that the magnitude of the change in the dipole moment of the ligand upon adsorption is correlated with the reduction of hot electron lifetime, and concluded that the perturbation of the lifetimes was electronic in nature.[44] A change in dipole moment is probably indicative of electronic mixing and a change in the interfacial DOS. Aruda *et al.*[42] determined, through transient absorption spectroscopy, that additional electronic states at the Fermi level of small Au NPs, contributed upon ligand exchange from amines to thiolates, increases the electronic heat capacity of the system, and leads to an increase in the hot electron lifetime upon photoexcitation.

Organic molecules can also affect the hot electron cooling rate by changing the rate of energy transfer between electrons and phonons – that is, the electron–phonon coupling magnitude. The electron–phonon coupling depends on (i) the density of electronic states of the NP system near the Fermi level[50] (like the electronic heat capacity), and (ii) the number and energetic distribution of available vibrational modes.[33,50] The electron–phonon coupling ($g(T_e)$) is therefore also sensitive to the surface chemistry of the NP through eqn (7), where $\langle\omega^2\rangle$ is the second moment of the

$$g(T_e) = \frac{\pi\hbar k_B \lambda \langle\omega^2\rangle}{\mathrm{DOS}(\varepsilon_{\mathrm{fermi}})} \int_{-\infty}^{\infty} \frac{df(\varepsilon, \mu, T_e)}{d\varepsilon} \mathrm{DOS}^2(\varepsilon) d\varepsilon \qquad (7)$$

phonon spectrum, and λ is the electron–phonon mass enhancement parameter (the change in effective mass of a carrier due to electron–phonon coupling). Both parameters are material dependent, and are often assumed to be bulk values without further justification.[31,50] The electron–phonon coupling has recently been shown to depend on (i) the electronic temperature of the system for both bulk metals and nanoparticles,[11,12,42,51]

(ii) the adsorption of ligands, which introduce high-energy vibrational modes (relative to lattice modes) to the NP system[39] and (iii) changes to the crystallinity of the system.[52] Huang *et al.* showed that, upon removing lattice defects in Au NPs and the associated high-energy vibrational modes, the electron–phonon coupling and the hot electron cooling rate decrease.[53] Aikens and coworkers have found that the adsorption of ligands on small metal clusters warps the crystal structure of the cluster,[52] and changes hot electron cooling lifetimes by altering both the available phonon modes in the NP and the associated electron–phonon coupling magnitudes.

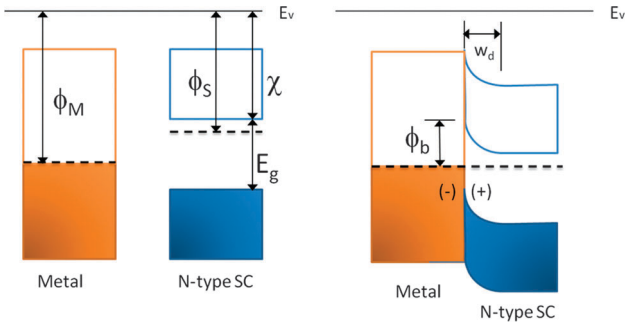

Fig. 2 A band diagram of a metal and a semiconductor, before (left) and after (right) formation of the metal–semiconductor Schottky junction. The diagram shows work functions for the metal (Φ_M) and semiconductor (Φ_S) (*versus* the vacuum energy E_v), the semiconductor electron affinity (χ), and the Schottky barrier ($\Phi_b = \Phi_M - \chi$). E_g is the band gap of the semiconductor, and W_d is the depletion width.

Observation of charge transfer-like interactions at the metal/semiconductor interface

Metal–semiconductor (M/SC) interactions are apparent in both steady state and time-resolved optical spectra of the two components. Studies of plasmon–exciton coupling and charge transfer phenomena in hybrid metal–semiconductor NPs are complicated by the wide variety of interfaces available. In some cases, a linker molecule separates the NP and semiconductor materials, while in others, the metal and semiconductor components are in direct contact. These composite materials therefore have a range of plasmon–exciton couplings. M/SC hybrids mostly fall into the weak-coupling category. For example, Gao *et al.*[55] report an extinction spectrum of hybrid Au/CdSe NPs synthesized *via* a seeded growth approach where the excitonic absorption due to the QDs is evident as a weak shoulder barely exceeding the broad, intense absorption from the plasmonic Au NPs. Similar extinction properties are observed by Neretina and co-workers.[56] Single QDs coupled to metallic NP dimers are predicted to exhibit exotic optical properties, such as narrow transparency induced by Fano interference and hybridization as a result of strong plasmon–exciton coupling, but such systems have yet to be experimentally realized.[57]

In experimental reports of M/SC hybrid systems, plasmon–exciton coupling effects manifest most strongly in their impact on relaxation processes in the system. Neretina and co-workers observed an anomalously large increase (as compared to expectations from Fermi's Golden Rule) in the intraband relaxation rate of CdTe nanowires coated with Au-nanoshells, for pump wavelengths resonant with Au nanoshell's localized surface plasmon resonance (LSP).[56] Both energy and charge transfer mechanisms are posited as explanations for this increase. A number of studies also note an increase in the exciton population decay rate of QD photon emitters in presence of a plasmonic nanostructure.[56,58,59] When exciting the LSP, additional pathways for energy dissipation become available.[56] In each case, the initial excitation of a LSP results in the transfer of energy to the QD, either by re-exciting cold conduction band electrons or creating additional excitons. In the case of strong exciton–plasmon coupling, an exciton can be annihilated resulting in the creation of an LSP in the plasmonic nanostructure.[60]

Electron transfer can occur from the metallic conduction band to the QD conduction band, provided the electronic structure of the hybrid material is appropriate. Both the chemistry and physics of the interface between metal and semiconductor are important, as not all M/SC interfaces are chemisorbed interfaces, and while Schottky junctions *can* form in nanomaterials,[61,62] rectifying potentials do not always form[63] at the M/SC interface. It is worthwhile to stress the importance of the preparation route on the surface chemistry and M/SC interface of the nanomaterials, as metal–semiconductor pairs that may form Schottky junctions in bulk materials may not form rectifying junctions on the nanoscale. There are a variety of reasons that a Schottky junction does not form, such as Fermi-level pinning at surface states; these reasons are outlined in a review by Léonard *et al.*[64] In the absence of surface chemistry-induced trap states, a rectifying junction, as seen in Fig. 2, is created at the M/SC interface due to charge transfer between the metal and semiconductor nanoparticles, which equilibrates the Fermi level of the metal and semiconductor. In ref. 58, Nikoobakht and co-workers attribute the quenching of QD photoluminescence to electron transfer from sub-Fermi orbitals in the gold to deep trap states in the QD.[58] Gao *et al.* exploit electron transfer processes in similar hybrid structures.[55] In their study, photoexcited QDs transfer a hot electron to the gold nanostructure, a process which is detected by fluorescent electron acceptor molecules. Simultaneously, a hole scavenging molecule was used to remove the hole from the QD. Extremely long retention times for the electron in the Au nanostructure were observed, inviting applications in charge harvesting and photocatalysis.

Direct photoinduced electron transfer (PET) from metal NPs into semiconductor domains is a well-documented phenomenon for Au–TiO_2 complexes, and has been proposed for other hybrid materials, such as core–shell Ag–Cu_2O[65] NPs and Au–Fe_2O_3 hybrid nanorods.[66–69] The main evidence for PET from metal to semiconductor is changes in the spectroscopic features of the free carriers in the semiconductor component upon photoexcitation of the metal component. Changes in the dynamics of plasmon recovery in the metal component have not been used as a diagnostic tool, because reported time constants for such PET are faster than the instrument response, so decay of the plasmon bleach due to PET will not be detected. An alternative

route to detect PET in these systems is to monitor the shift in the position of the transient bleach of the plasmon (with respect to its steady-state peak position); the plasmon frequency increases with the square root of the density of charge carriers in the NP.

Tachiya and coworkers observed growth of an IR signal due to intraband transitions of TiO_2 following excitation of Au NPs in contact with the semiconductor.[29,70,71] Control experiments using a dye–TiO_2 system with unity PET efficiency and Au/ZrO_2 confirmed the assignment of the IR signal increased charge density due to PET from the metal. The authors reported an efficiency of 0.4% for charge separation with approximately 1000 photons absorbed per Au NP.[70] In a thermalized hot-electron population, very few electrons per NP (fewer than ten for a 10 nm Au NP excited by a thousand 532 nm photons) will have enough energy to surpass the Schottky barrier of the Au–TiO_2 system (which is around 1.0 eV[70]), which suggests that Au-to-TiO_2 PET may occur from a non-thermalized electron state. This conclusion is supported by the fact that Tachiya *et al.* report a PET time constant <50 fs, while the timescale for hot electron thermalization is $\sim$100 fs. The application of Au NP/TiO_2 in solar cells is limited by the nanosecond charge-recombination time constant. The authors proposed that charge recombination can be slowed either by avoiding the saturation of electron traps in TiO_2 by using low-energy excitation, or by increasing the size of TiO_2 particles. Increasing the size of the particle increases the charge recombination time constant because the electron should diffuse and explore the whole TiO_2 particle in order to find the hole in the Au NP and recombine.[70]

A recent study of Ag–Cu_2O core–shell NPs revealed both PET and plasmon-induced resonant energy transfer from the Ag core into the Cu_2O shell.[71] The dynamics of the system following selective photoexcitation of the Ag core were probed at a wavelength of 800 nm, whose dynamics has contributions from both the Ag plasmon and the Cu_2O free carriers. The transient signal at 800 nm showed a long-lived component (>10 ps) that was attributed to photoelectrons transferred from the Ag core into the Cu_2O shell. Spectral overlap between the Ag plasmon and the Cu_2O free carrier signals prevented the quantification of the PET timescale, since, at delay times shorter than one picosecond, the ultrafast transient absorption (TA) signal was dominated by the bleach of the Ag plasmon peak.

Comin, Korobchevskaya *et al.* studied the TA dynamics of Au–Fe_2O_3 nanohybrids with different morphologies (dumbbell-like and rod-like Au–Fe_2O_3, see Fig. 3C and D, respectively) exciting both the Au and the Fe_2O_3 components.[66,67,69] In the case of rod-like Au–Fe_2O_3 nanohybrids, the position of the plasmon transient bleach was shifted with respect to the position of the ground-state absorption peak, which suggests an increase in the electron density of the Au domain within the first 100 fs after photoexcitation. No difference between the ground-state and the transient plasmon peak positions was observed for dumbbell-like Au–Fe_2O_3 nanohybrids. The authors suggested that photoinduced charge separation occurs in rod-like Au–Fe_2O_3 but not in dumbbell-like Au–Fe_2O_3 due to the higher density of traps in the former, as a result of the synthetic protocol.[68] Interestingly, it does not appear that the PET process affects the decay rate of hot electrons in the metal component.

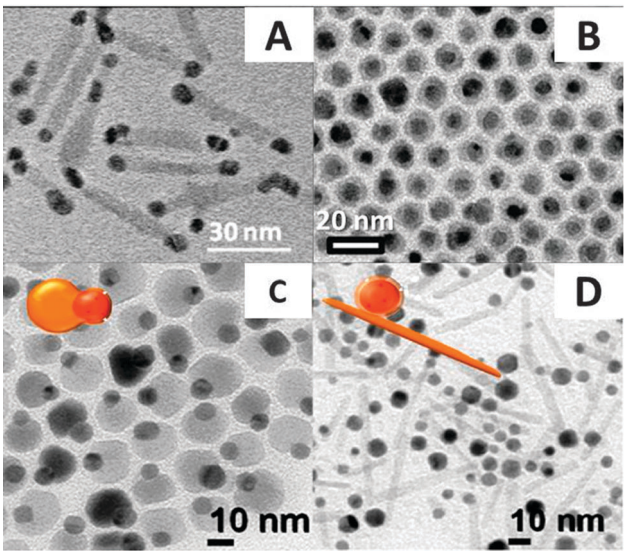

Fig. 3 TEM images of (A) gold-tipped CdS nanorods,[72] (B) core@shell Au@PbS nanoparticles,[74] (C) dumbbell-like Fe_2O_3–Au nanoparticles and (D) rod-like Fe_2O_3–Au hybrids.[66,67] The Au component is darker than the SC materials in all images.

Khon *et al.*[72] observed that the ground-state plasmon peak is suppressed in Au-tipped CdS nanorods (TEM images reproduced in Fig. 3), and attributed this result to the delocalization of the Au electrons into the CdS component. This result suggests very strong charge-transfer-like coupling between the Au and the CdS domain. Moreover, the TA spectrum following photoexcitation of both the Au and CdS components showed photoinduced absorption at the plasmon wavelength instead of the expected plasmon bleach observed for pure Au NPs, which was attributed to the formation of trap states at the CdS–Au interface (Fig. 4). Selective excitation of the Au component was not addressed in this study and other reports on Au-tipped CdS did not reproduce the novel spectroscopic features reported in this work.[73] Further work is therefore necessary to determine whether and to what extent delocalization of the Au electrons into the CdS component occurs in Au-tipped CdS nanorods, in the ground state and following photoexcitation.

Charge separation at the metal–semiconductor interface is well-documented in Au–TiO_2 composites. In the cases of core–shell Ag–Cu_2O and rod-like Au–Fe_2O_3, spectral overlap between metal and semiconductor absorption bands complicates the analysis. It is interesting to note that none of the semiconductor particles acting as electron acceptors in these studies have sizes in the quantum-confined regime, so there is opportunity to investigate PET from metal NPs to semiconductor QDs. The size-dependent energy levels in QDs facilitate the study of the dependence of PET and charge recombination rate on driving force. Another interesting research direction involves replacing the Au NPs by nanorods in order to shift the plasmon resonance to lower energy, and thus study the dependence of the PET efficiency on the energy of the incident photons. These fundamental studies are important for expanding the regime of the solar spectrum that will be accessible for solar cells in which plasmonic NPs serve as the active material, and

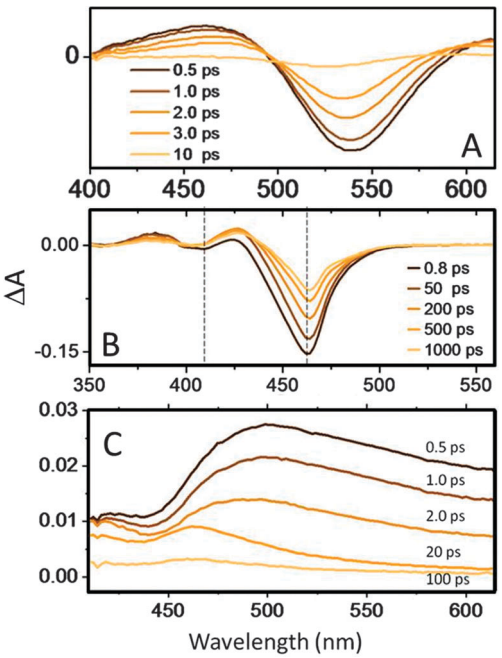

Fig. 4 TA spectra of 5.3 nm Au NPs (upper panel), CdS nanorods (middle panel) and Au tipped CdS nanorods (lower panel). Reproduced from ref. 72.

for determining whether PET occurs from a thermalized state. The PET efficiency from a thermalized electron population depends only on the total energy deposited in the nanoparticle, regardless of the total photon energy (*i.e.* a 400 nm photon will have the same effect than two 800 nm photons), whereas PET from a non-thermalized population is expected to be highly dependent on the energy of individual photons.

Applications of explicit charge transfer with metal nanoparticles as electron donors

Charge extraction from photoexcited metal NPs has been used to produce photocurrent in metal NP–semiconductor systems and to enable photocatalysis at the metal–small molecule interface. The presence of photoinduced charge separation is well documented by these experiments; however, several open questions exist: (i) the state of the electron population that participates in CT in these examples is unknown; this state may be either a coherent state, a completely decohered but non-thermalized state or completely thermalized state. (ii) The rate constants for the electron transfer in most of these systems have not been determined and therefore the magnitude of the donor–acceptor coupling is poorly understood. It is not yet clear whether the charge-separated state is optically accessible, or whether charge transfer is achieved through local excitation followed by charge separation. (iii) The observation of photocurrents and photocatalysis suggests that charge recombination is slow or incomplete, but there is need to study the kinetics of charge recombination and its role in determining the efficiency of energy conversion. Below, we discuss several examples of explicit charge transfer between metal NPs and molecular or semiconductor acceptors.

Weak photocurrents have been observed in citrate stabilized metal NP films on ITO electrodes.[48] The authors submit that the photovoltage is due to irreversible oxidation of the adsorbed citrate by hot holes in metal NPs irradiated at the LSP absorption. The photocurrent produced in Au NPs is much less than in Ag NPs, even though the driving force for hole transfer is larger. The authors propose, therefore, that CT may occur in the Marcus inverted region; however, CT in the inverted region is unlikely when the donor is a thermalized electron distribution. The observed difference between rates of CT from Ag and Au may instead be due to differences in the electronic coupling between the metal and citrate. The results of this study are encouraging because the existence of photocurrent demonstrates that the charge injection rates into organic molecules can be competitive with the intrinsic decay pathways of photogenerated carriers in metal NPs.

In addition to the TA studies referenced in the previous section, charge injection from Au NPs into TiO_2 has been observed through the generation of photovoltage in a device.[29,63,75,76] After photon absorption, energetic electrons are generated by plasmon decay, and are transported to and injected over what is described as a Schottky barrier. Charge injection from Au NPs into TiO_2 has the highest efficiency of the charge-transfer examples listed in this section, and confirms that charge transfer across the Schottky junction is competitive with hot electron cooling.[77] There are many well-designed experiments that demonstrate the feasibility and mechanism of electron transfer in this system. Zhao *et al.* were the first to show the effect (although with a very low incident photon to current conversion efficiency, IPCE), using a sol–gel synthesis of Au and Ag NPs on a TiO_2 film.[76] The authors increased the stability and IPCE of this system (to 26%) by adding an optimized electron mediator ($Fe^{2+/3+}$), which shuttles electrons from TiO_2 to the counter electrode.[63,75] Fermi level pinning at M/SC interfaces is sometimes observed.[64] Since the mechanism for charge transfer requires hot carrier emission over the Schottky barrier, Fermi level pinning is detrimental to this process.

Another application of photoinduced charge separation in metal NP systems is the synthesis of anisotropic NPs by photoirradiation, first published by Mirkin and coworkers.[78] The final shape and size of these silver and gold nanoprisms depends on the wavelength of light used during the synthesis. The proposed mechanism suggests electron transfer from a photoirradiated metal seed to Au or Ag ions in solution. This process is more efficient at the plasmonic hot spots on the metallic NP than in other parts of the surface; therefore, the shape of the resulting nanoparticle is dictated by its plasmon spectrum, and, in turn, its size and shape. A recent paper by Schatz *et al.* modeled this reaction by studying the electron transfer reaction between a silver cluster and a silver ion.[79] Time-dependent Density Functional Theory was used to calculate the charge transfer rates from a small silver cluster to a silver ion at a varied distance. The net yield of CT, which is in competition with plasmon dissipation, is very small, a result that is in qualitative agreement with the slow (day-long) growth kinetics of the Au NPs. Charge transfer from a coherent plasmonic state in a NP of several nanometers may be larger than that calculated for the cluster due to the presence of

multiple charge donors in the NP and the strong electric fields generated in the vicinity of the NP by the plasmon resonance. Nevertheless, the theoretical analysis highlights that small electronic coupling between the metal NP and the electron acceptor and ultrafast energy dissipation of the hot electrons in the metal NP are the main challenges for efficient charge extraction from plasmonic NPs.

Recent reports on the use of plasmons to enable reactions involving hydrogen and water open new possibilities for highly stable photocatalysts with strong tunable absorptions over the visible spectrum. Halas and coworkers report the dissociation of di-hydrogen and di-deuterium adsorbed on the surface of Au NPs after plasmonic excitation to form H–D.[80] The proposed mechanism for dissociation of dihydrogren is transient occupation of the antibonding orbital of dihydrogen with a plasmonically excited electron from the Au NP, which is similar to the ultrafast chemical interface scattering mechanism described earlier. In a second example, Moskovits and coworkers report the production of oxygen and hydrogen from water by using Au nanorods as the source for electrons, and a platinum NP as the catalytic surface.[81] The authors designed the photocatalytic cell with a thin layer of TiO_2 as a hole blocking layer that would allow electron transfer to the Pt catalyst, and reduce charge recombination; however, the authors observed a decrease in the photocatalytic yield with increasing TiO_2 thickness. Note that the TiO_2 layer will form a Schottky junction, which will enhance charge separation, but the hot electrons still must diffuse through the TiO_2 to the Pt catalyst in order to split water. This system has much room for further optimization at the M/SC interface, and has potential to have notable efficiency for water splitting.

Conclusion

Competition between CT and energy dissipation have so far limited the magnitude of photocurrent and yield of photocatalysis originating from charge carriers created by excitation of plasmons in metal NPs. Isolated plasmonic NPs dissipate energy on the femtosecond timescale through hot electron cooling, but we are learning to control this dissipation by engineering the electronic structure of the interface between the metal particle and its surrounding matrix. Examples of charge transfer from Au NPs to TiO_2 have shown the highest efficiency of charge transfer so far, and served as a demonstration that fast charge extraction can out-compete dissipation. Ongoing research on the mechanisms by which interfacial chemistry dictates electron dynamics in metal NPs will push this field toward technological applications of multi-electron excited states in these complicated systems.

Notes and references

1 H. A. Atwater and A. Polman, *Nat. Mater.*, 2010, **9**, 205–213.
2 C. Bauer, J.-P. Abid and H. H. Girault, *J. Phys. Chem. B*, 2006, **110**, 4519–4523.
3 L. Brus, *Acc. Chem. Res.*, 2008, **41**, 1742–1749.
4 M. A. El-Sayed, *Acc. Chem. Res.*, 2004, **37**, 326–333.
5 C. Bauer, J.-P. Abid, D. Fermin and H. H. Girault, *J. Chem. Phys.*, 2004, **120**, 9302–9315.
6 C. Bauer, J.-P. Abid and H. H. Girault, *Chem. Phys.*, 2005, **319**, 409–421.
7 C. Bauer, J.-P. Abid and H. H. Girault, *C. R. Chim.*, 2006, **9**, 261–267.
8 X. Liu, M. Atwater, J. Wang and Q. Huo, *Colloids Surf., B*, 2007, **58**, 3–7.
9 G. V. Hartland, *Phys. Chem. Chem. Phys.*, 2004, **6**, 5263–5274.
10 C. Novo, D. Gomez, J. Perez-Juste, Z. Zhang, H. Petrova, M. Reismann, P. Mulvaney and G. V. Hartland, *Phys. Chem. Chem. Phys.*, 2006, **8**, 3540–3546.
11 W. S. Fann, R. Storz, H. W. K. Tom and J. Bokor, *Phys. Rev. Lett.*, 1992, **68**, 2834–2837.
12 J. P. Girardeau-Montaut and C. Girardeau-Montaut, *Phys. Rev. B: Condens. Matter Mater. Phys.*, 1995, **51**, 13560–13567.
13 R. H. M. Groeneveld, R. Sprik and A. Lagendijk, *Phys. Rev. B: Condens. Matter Mater. Phys.*, 1995, **51**, 11433–11445.
14 T. S. Ahmadi, S. L. Logunov and M. A. El-Sayed, *J. Phys. Chem.*, 1996, **100**, 8053–8056.
15 S. L. Logunov, T. S. Ahmadi, M. A. El-Sayed, J. T. Khoury and R. L. Whetten, *J. Phys. Chem. B*, 1997, **101**, 3713–3719.
16 J. H. Hodak, I. Martini and G. V. Hartland, *J. Phys. Chem. B*, 1998, **102**, 6958–6967.
17 H. Inouye, K. Tanaka, I. Tanahashi and K. Hirao, *Phys. Rev. B: Condens. Matter Mater. Phys.*, 1998, **57**, 11334–11340.
18 L. Jiang and H.-L. Tsai, *J. Heat Transfer*, 2005, **127**, 1167–1173.
19 R. Rosei, F. Antonang and U. M. Grassano, *Surf. Sci.*, 1973, **37**, 689–699.
20 U. Kreibig and M. Vollmer, *Optical Properties of Metal Clusters*, Springer, 1995.
21 C. Sönnichsen, T. Franzl, T. Wilk, G. von Plessen, J. Feldmann, O. Wilson and P. Mulvaney, *Phys. Rev. Lett.*, 2002, **88**, 077402.
22 C. Sönnichsen, T. Franzl, T. Wilk, G. v. Plessen and J. Feldmann, *New J. Phys.*, 2002, **4**, 93.
23 F. Stietz, J. Bosbach, T. Wenzel, T. Vartanyan, A. Goldmann and F. Träger, *Phys. Rev. Lett.*, 2000, **84**, 5644–5647.
24 R. A. Molina, D. Weinmann and R. A. Jalabert, *Phys. Rev. B: Condens. Matter Mater. Phys.*, 2002, **65**, 155427.
25 C. Dahmen, B. Schmidt and G. von Plessen, *Nano Lett.*, 2007, **7**, 318–322.
26 M. Liu, M. Pelton and P. Guyot-Sionnest, *Phys. Rev. B: Condens. Matter Mater. Phys.*, 2009, **79**, 035418.
27 D. Charles, M. Gara, D. Aherne, D. Ledwith, J. Kelly, W. Blau and M. Brennan-Fournet, *Plasmonics*, 2011, **6**, 351–362.
28 C. Bauer, J.-P. Abid, D. Fermin and H. H. Girault, *J. Chem. Phys.*, 2004, **120**, 9302–9315.
29 A. Furube, L. Du, K. Hara, R. Katoh and M. Tachiya, *J. Am. Chem. Soc.*, 2007, **129**, 14852–14853.
30 B. A. Smith, J. Z. Zhang, U. Giebel and G. Schmid, *Chem. Phys. Lett.*, 1997, **270**, 139–144.
31 S. Link, C. Burda, Z. L. Wang and M. A. El-Sayed, *J. Chem. Phys.*, 1999, **111**, 1255–1264.
32 J. Y. Bigot, V. Halté, J. C. Merle and A. Daunois, *Chem. Phys.*, 2000, **251**, 181–203.

33 A. Arbouet, C. Voisin, D. Christofilos, P. Langot, N. D. Fatti, F. Vallée, J. Lermé, G. Celep, E. Cottancin, M. Gaudry, M. Pellarin, M. Broyer, M. Maillard, M. P. Pileni and M. Treguer, *Phys. Rev. Lett.*, 2003, **90**, 177401.
34 M. Hu and G. V. Hartland, *Hot Adsorbate-Induced Retardation of the Internal Thermalization of Nonequilibrium Electrons in Adsorbate-Covered Metal Nanoparticles*, 2002, **106**, 7029–7033.
35 S. Link, A. Furube, M. B. Mohamed, T. Asahi, H. Masuhara and M. A. El-Sayed, *J. Phys. Chem. B*, 2002, **106**, 945–955.
36 S. Link, D. J. Hathcock, B. Nikoobakht and M. A. El-Sayed, *Adv. Mater.*, 2003, **15**, 393–396.
37 M. Perner, P. Bost, U. Lemmer, G. von Plessen, J. Feldmann, U. Becker, M. Mennig, M. Schmitt and H. Schmidt, *Phys. Rev. Lett.*, 1997, **78**, 2192–2195.
38 T. S. Ahmadi, S. L. Logunov and M. A. El-Sayed, *J. Phys. Chem.*, 1996, **100**, 8053–8056.
39 J. S. Melinger, V. D. Kleiman, D. McMorrow, F. Gröhn, B. J. Bauer and E. Amis, *J. Phys. Chem. A*, 2003, **107**, 3424–3431.
40 A.-M. Dowgiallo and K. L. Knappenberger, *Phys. Chem. Chem. Phys.*, 2011, **13**, 21585–21592.
41 R. D. Averitt, S. L. Westcott and N. J. Halas, *J. Opt. Soc. Am. A*, 1999, **16**, 1814–1823.
42 K. O. Aruda, M. Tagliazucchi, C. M. Sweeney, D. C. Hannah, G. C. Schatz and E. A. Weiss, *Proc. Natl. Acad. Sci. U. S. A.*, 2013, **110**, 4212–4217.
43 M. Nakamura, K. Tamura, S. Murakami, Y. E. N. Wen-Hsing, H. Suga and T. Ozawa, *Thermochim. Acta*, 1995, **253**, 127–136.
44 S. L. Westcott, R. D. Averitt, J. A. Wolfgang, P. Nordlander and N. J. Halas, *J. Phys. Chem. B*, 2001, **105**, 9913–9917.
45 S. K. Ghosh and T. Pal, *Phys. Chem. Chem. Phys.*, 2009, **11**, 3831–3844.
46 A. N. Caruso, L. G. Wang, S. S. Jaswal, E. Y. Tsymbal and P. A. Dowben, *J. Mater. Sci.*, 2006, **41**, 6198–6206.
47 P. Lakshminarayana and X. Qing-Hua, *Nanotechnology*, 2009, **20**, 185606.
48 X. Wu, E. S. Thrall, H. Liu, M. Steigerwald and L. Brus, *J. Phys. Chem. C*, 2010, **114**, 12896–12899.
49 P. K. Jain, W. Qian and M. A. El-Sayed, *J. Am. Chem. Soc.*, 2006, **128**, 2426–2433.
50 Z. Lin, L. V. Zhigilei and V. Celli, *Phys. Rev. B: Condens. Matter Mater. Phys.*, 2008, **77**, 075133.
51 J. K. Chen and J. E. Beraun, *J. Opt. A: Pure Appl. Opt.*, 2003, **5**, 168.
52 M. Zhu, C. M. Aikens, F. J. Hollander, G. C. Schatz and R. Jin, *J. Am. Chem. Soc.*, 2008, **130**, 5883–5885.
53 W. Huang, W. Qian, M. A. El-Sayed, Y. Ding and Z. L. Wang, *J. Phys. Chem. C*, 2007, **111**, 10751–10757.
54 M. Busby, C. Chiorboli and F. Scandola, *J. Phys. Chem. B*, 2006, **110**, 6020–6026.
55 B. Gao, Y. Lin, S. Wei, J. Zeng, Y. Liao, L. Chen, D. Goldfeld, X. Wang, Y. Luo, Z. Dong and J. Hou, *Nano Res.*, 2012, **5**, 88–98.
56 S. Neretina, W. Qian, E. Dreaden, M. A. El-Sayed, R. A. Hughes, J. S. Preston and P. Mascher, *Nano Lett.*, 2008, **8**, 2410–2418.
57 X. Wu, S. K. Gray and M. Pelton, *Opt. Express*, 2010, **18**, 23633–23645.
58 B. Nikoobakht, C. Burda, M. Braun, M. Hun and M. A. El-Sayed, *Photochem. Photobiol.*, 2002, **75**, 591–597.
59 S. H. Choi, B. Kwak, B. Han and Y. L. Kim, *Opt. Express*, 2012, **20**, 16785–16793.
60 K. H. An, M. Shtein and K. P. Pipe, *Opt. Express*, 2010, **18**, 4041–4048.
61 S. W. Boettcher, N. C. Strandwitz, M. Schierhorn, N. Lock, M. C. Lonergan and G. D. Stucky, *Nat. Mater.*, 2007, **6**, 592–596.
62 B. A. Korgel, *Nat. Mater.*, 2007, **6**, 551–552.
63 V. Subramanian, E. E. Wolf and P. V. Kamat, *J. Am. Chem. Soc.*, 2004, **126**, 4943–4950.
64 F. Léonard and A. A. Talin, *Nat. Nanotechnol.*, 2011, **6**, 773–783.
65 J. Li, S. K. Cushing, J. Bright, F. Meng, T. R. Senty, P. Zheng, A. D. Bristow and N. Wu, *ACS Catal.*, 2012, **3**, 47–51.
66 K. Korobchevskaya, C. George, L. Manna and A. Comin, *J. Phys. Chem. C*, 2012, **116**, 26924–26928.
67 A. Comin, K. Korobchevskaya, C. George, A. Diaspro and L. Manna, *Nano Lett.*, 2012, **12**, 921–926.
68 C. George, A. Genovese, F. Qiao, K. Korobchevskaya, A. Comin, A. Falqui, S. Marras, A. Roig, Y. Zhang, R. Krahne and L. Manna, *Nanoscale*, 2011, **3**, 4647–4654.
69 K. Korobchevskaya, C. George, A. Diaspro, L. Manna, R. Cingolani and A. Comin, *Appl. Phys. Lett.*, 2011, **99**, 011907.
70 L. Du, A. Furube, K. Yamamoto, K. Hara, R. Katoh and M. Tachiya, *J. Phys. Chem. C*, 2009, **113**, 6454–6462.
71 L. Du, A. Furube, K. Hara, R. Katoh and M. Tachiya, *Thin Solid Films*, 2009, **518**, 861–864.
72 E. Khon, A. Mereshchenko, A. N. Tarnovsky, K. Acharya, A. Klinkova, N. N. Hewa-Kasakarage, I. Nemitz and M. Zamkov, *Nano Lett.*, 2011, **11**, 1792–1799.
73 D. Mongin, E. Shaviv, P. Maioli, A. Crut, U. Banin, N. Del Fatti and F. Vallée, *ACS Nano*, 2012, **6**, 7034–7043.
74 Y. Kobayashi, Y. Nonoguchi, L. Wang, T. Kawai and N. Tamai, *J. Phys. Chem. Lett.*, 2012, **3**, 1111–1116.
75 Y. Tian and T. Tatsuma, *J. Am. Chem. Soc.*, 2005, **127**, 7632–7637.
76 G. Zhao, H. Kozuka and T. Yoko, *Thin Solid Films*, 1996, **277**, 147–154.
77 M. W. Knight, H. Sobhani, P. Nordlander and N. J. Halas, *Science*, 2011, **332**, 702–704.
78 C. Xue, J. E. Millstone, S. Li and C. A. Mirkin, *Angew. Chem.*, 2007, **119**, 8588–8591.
79 H. Chen, M. A. Ratner and G. C. Schatz, *J. Phys. Chem. C*, 2012.
80 S. Mukherjee, F. Libisch, N. Large, O. Neumann, L. V. Brown, J. Cheng, J. B. Lassiter, E. A. Carter, P. Nordlander and N. J. Halas, *Nano Lett.*, 2012, **13**, 240–247.
81 S. Mubeen, J. Lee, N. Singh, S. Kramer, G. D. Stucky and M. Moskovits, *Nat. Nanotechnol.*, 2013, **8**, 247–251.